compounds

MDPI

Article

Donepezil Derivatives as Potential Dual AChE/BChE Inhibitors: Fragment-Based Design, AI-Assisted Retrosynthesis, and *In Silico* Evaluation

Marko Antonijević [1,*], Jelena Đorović Jovanović [1,*], Marijana Stanojević Pirković [2], Miona Glišić [3], Ana Antonijević [4] and Svetlana Jeremić [5]

1 Institute for Information Technologies, University of Kragujevac, 34000 Kragujevac, Serbia
2 Department of Medical Biochemistry, Faculty of Medical Sciences, University of Kragujevac, 34000 Kragujevac, Serbia; marijanas14@gmail.com
3 Department of Dentistry, Faculty of Medical Sciences, University of Kragujevac, 34000 Kragujevac, Serbia; mionagrujovic@yahoo.com
4 Faculty of Metallurgy and Technology, University of Montenegro, Džordža Vašingtona bb, 81000 Podgorica, Montenegro; antonijevic.ana997@gmail.com
5 Department of Natural and Mathematical Science, State University of Novi Pazar, Vuka Karadžića bb, 36300 Novi Pazar, Serbia; sjeremic@np.ac.rs
* Correspondence: mantonijevic@uni.kg.ac.rs (M.A.); jelena.djorovic@uni.kg.ac.rs (J.Đ.J.)

Abstract

Alzheimer's disease (AD) is a complex neurodegenerative condition marked by a gradual decline in cognitive abilities, a reduction in acetylcholine (ACh) levels, and the accumulation of β-amyloid (Aβ) plaques. In a healthy brain, approximately 80% of ACh is broken down by acetylcholinesterase (AChE). Meanwhile, butyrylcholinesterase (BChE) serves a supportive function, gaining significance as AChE activity diminishes during the progression of Alzheimer's disease. Modern therapeutic approaches focus on creating dual inhibitors of AChE and BChE that also aim to diminish Aβ-amyloidogenesis through interactions with the peripheral anionic site (PAS). This study combined fragment-based molecular design (CReM), AI-assisted retrosynthetic feasibility assessment, and in silico evaluation (docking, molecular dynamics, and ADMET profiling) to identify novel Donepezil derivatives as potential dual AChE/BChE inhibitors. A series of 10,000 derivatives were developed through computational methods and carefully assessed based on stringent drug-likeness, synthetic accessibility, and medicinal chemistry standards. This was succeeded by comprehensive ADMET profiling. Nine candidates were identified with predicted CNS pharmacokinetics, adequate toxicological profiles and reduced cytochrome P450 liabilities. Molecular docking yielded improved predicted binding affinities relative to Donepezil. Several derivatives, particularly **D4** and **D5**, showed dual-site binding poses spanning both the catalytic gorge and the PAS. MD simulations indicated the stability of these poses over 100 ns. These computational results suggest that the proposed derivatives may preserve or improve upon Donepezil's pharmacokinetic profile while offering potentially balanced AChE/BChE inhibition and anti-amyloidogenic activity, pending experimental validation.

Keywords: Alzheimer's disease; Donepezil; AChE inhibitor; BChE inhibitor; CReM; molecular dynamics

Check for updates

Academic Editors: Małgorzata Anna Marć, Enrique Domínguez-Álvarez and Alcides Pinto Simao

Received: 2 June 2026
Revised: 18 July 2026
Accepted: 23 July 2026
Published: 24 July 2026

Copyright: © 2026 by the authors. Licensee MDPI, Basel, Switzerland. This article is an open access article distributed under the terms and conditions of the Creative Commons Attribution (CC BY) license.

1. Introduction

Alzheimer's disease (AD) is a neurodegenerative disorder that occurs as a result of synaptic dysfunctions and the destruction of neurons in the cerebral cortex, leading to the loss of overall brain mass. The development of Alzheimer's disease results in severe memory loss, particularly short-term memory, reduced cognitive abilities, and significant behavioural changes, such as the onset of depression, loss of interest in activities, lack of trust in others, sleep disturbances, and more [1]. The occurrence of Alzheimer's disease is prevalent among the elderly population. As the proportion of elderly individuals increases each year, the impact of this disease has grown to epidemic proportions. Although genetics is considered the primary risk factor for the development of this disease [2], some studies have shown that a diet high in fats, which also contributes to high blood pressure, atherosclerosis, and elevated cholesterol levels, also increases the risk of developing Alzheimer's disease [3]. Another contributing factor, as suggested by certain analyses, is environmental influence, which in some cases has led to increased levels of aluminium in brain cells [4], or poisoning from organophosphates and carbamates [5]. Additionally, analysis of medical records from World War II veterans who experienced moderate or severe head injuries in their youth revealed a higher incidence of the disease in this group [6].

During the analysis of the causes and consequences of the onset of Alzheimer's disease, it was concluded that the reduction in the ability to learn and remember in patients suffering from this disease occurs as a result of a decrease in the level and function of the neurotransmitter acetylcholine (ACh) in the central nervous system [7]. It was found that in a healthy brain, about 80% of ACh is degraded by acetylcholinesterase (AChE), while butyrylcholinesterase (BChE) plays an additional, supportive role, primarily contributing to ACh hydrolysis when AChE activity is reduced or impaired. With the progression of AD, the activity of AChE decreases naturally (or by using AChE inhibitors such as Donepezil), while the importance of BChE in the process of ACh degradation becomes more significant [8–10].

By studying the changes occurring in the brain tissue of AD patients, the occurrence of Aβ amyloidogenesis was observed [11]. This phenomenon implies that soluble oligomers of β-amyloid peptide (Aβ) are formed in the early stages of AD development, which with the progression of the disease first form a fibrous structure and then plaques of β-amyloid peptide (Aβ) [12,13]. It is also known that the peripheral anionic site (PAS) of the AChE enzyme can promote Aβ aggregation and the occurrence of Aβ-amyloidogenesis [14].

Therefore, the new trends in the development of drugs that are used to alleviate the symptoms of AD are focused on designing compounds that inhibit both AChE and BChE. Such compounds would contribute to slowing down the loss of cognitive functions of patients by preventing the degradation of the neurotransmitter ACh, while also inhibiting Aβ-amyloidogenesis [15].

Bearing in mind that the development of AD occurs as a result of multiple factors simultaneously, no way has yet been found to stop this disease. However, appropriate therapy can significantly alleviate symptoms and slow disease progression. In this study, a theoretical approach and the application of the CReM (Chemically Reasonable Mutations) webserver, ADMET analysis, and molecular docking protocols were used to generate the structure of a series of compounds, the potential dual inhibitors of AChE and BChE.

2. Materials and Methods

2.1. Generation of Donepezil Derivatives Using CReM

To improve the AD and neuroprotective effects of Donepezil, a series of around 10,000 structurally diverse derivatives was generated using the CReM webserver [16]. The parent molecule (Donepezil) was used as the reference scaffold, and modifications were

introduced at predefined substitution sites, focusing on positions that are not involved in crucial interactions with AChE. Mutations were restricted to transformations allowed by the default CReM fragment database to ensure chemical feasibility and synthetic accessibility. CReM is a fragment-based, context-driven generation method rather than a machine-learning model: it enumerates modifications by swapping fragments that occur in equivalent chemical contexts within a ChEMBL-derived database, which guarantees chemical validity by construction.

2.2. Filtering by Drug-Likeness and ADMET Criteria

Filtering was conducted according to druglikeness criteria, as well as considerations from medicinal chemistry such as PAINS (Pan-Assay Interference Compounds) and BRENK (BRENK's Structural Alerts) [17–19]. Additionally, synthetic accessibility was assessed with a threshold of $\leq$4.5, alongside the evaluation of the bioavailability score. Particular attention was directed towards properties that are significant for compounds aimed to be active in the CNS. This includes a high predicted gastrointestinal (GI) absorption, the ability to permeate the blood–brain barrier (BBB), and minimal interaction with P-glycoprotein (P-gp). These analyses were done using ADMETlab 3.0 [19] which offered a comprehensive prediction of oral bioavailability, plasma protein binding, hepatotoxicity, hERG-related cardiotoxicity, mutagenic and carcinogenic potential, along with CYP450 enzyme inhibition profiles. The molecules that met set criteria were subsequently reexamined with SwissADME [18]. We retained only those compounds that were predicted to exhibit excellent oral bioavailability and plasma distribution, alongside a low risk of liver and cardiac toxicity, and that raised no concerns regarding mutagenicity or carcinogenicity according to both webservers. Following the implementation of this thorough ADMET profiling approach, only nine derivatives fulfilled all the criteria and were chosen for additional computational assessment. Lastly, toxicological properties were considered as well, via ProTox 3.0 webserver [19]. SwissADME and ADMETlab 3.0 predictions were used as orthogonal in silico filters rather than definitive safety or pharmacokinetic evidence. When discrepancies between platforms occurred, the results were interpreted conservatively and reported separately. All the information from the SwissADME, ADMETlab 3.0 and ProTOX III can be found in the Supplementary Material.

2.3. Molecular Docking—Interactions with AChE and BChE

Selected compounds were further subjected to molecular docking simulations to investigate their inhibitory potential. Molecular docking studies were conducted utilizing AutoDock 4.2 via the AMDock graphical interface, focusing on both AChE and BChE [20,21]. The crystal structures of human AChE (PDB ID: 4EY7) and BChE (PDB ID: 7AIY) were obtained from the RCSB Protein Data Bank, with all crystallographic water molecules and heteroatoms removed during the preparation process [22,23]. During the preparation phase, polar hydrogens and Gasteiger charges were incorporated into the protein structures utilizing AutoDockTools (ADT) [20].

Ligand structures were generated in PDBQT format after undergoing energy minimization with the MMFF94 force field [24]. The docking process utilized the Lamarckian Genetic Algorithm (LGA), adhering to standard parameters that included 100 runs for each ligand, a population size of 150, a total of 2.5 million energy evaluations, and a cap of 27,000 generations [20]. The grid box was positioned at the center of the active site gorge of each enzyme, with dimensions designed to include the entire binding cavity. Grid was centered at x = 10.95, y = −56.55, and z = −23.47 with grid size 24 × 24 × 24 for AChE, and at x = −20.10, y = −14.86, and z = 41.45 with grid size 24 × 24 × 24 for BChE.

The analysis of docking outputs was conducted by examining binding affinity (kcal/mol), inhibition constant (Ki), and the clustering of conformations. The highest-scoring binding poses were visualized through Discovery Studio Visualizer to assess important interactions [25]. We conducted comparative docking using Donepezil and Donepezil derivative (*2-{1-[4-(12-Amino-3-chloro-6,7,10,11-tetrahydro-7,11-methanocycloocta[b]quinolin-9-yl)butyl]-1H-1,2,3-triazol-4-yl}-N-[4-hydroxy-3-methoxybenzyl]acetamide*)—**D0** [26,27] as the reference ligands for better understanding the binding affinity and interactions of the new derivatives. Ligand efficiency (LE) was computed by AMDock as

$$LE = \Delta G_{bind} / N_{heavy} \quad (1)$$

where ΔG_{bind} is the predicted binding free energy and N_{heavy} the number of non-hydrogen atoms [21,28]; the sign of ΔG_bind is retained, so more negative LE values indicate greater per-atom efficiency.

The docking protocol was validated by redocking the co-crystallized ligand of AChE (PDB 4EY7, donepezil), which reproduced the crystallographic pose with a heavy-atom RMSD of 1.96 Å, within the accepted 2 Å threshold.

2.4. Molecular Dynamics Simulations

Molecular dynamics simulations were performed for the two top-ranked derivatives, **D4** and **D5**, in complex with human AChE (PDB ID: 4EY7), using Donepezil as the reference. System preparation was carried out using CHARMM-GUI [29], with each protein–ligand complex embedded in an explicit TIP3P water box with a minimum distance of 10 Å between any protein atom and the box edge. Sodium and chloride ions were added to neutralize the system and establish a physiological salt concentration of 0.15 M. The AMBER ff14SB force field [30] was applied to the protein, while ligand parameters were generated using the General AMBER Force Field version 2 [31,32] with AM1-BCC partial charges assigned via the antechamber module of AmberTools22.

All simulations were conducted using AMBER 22 [33]. Prior to production runs, each system was subjected to a multi-stage equilibration protocol: (i) energy minimization with 2500 steps of steepest descent followed by 2500 steps of conjugate gradient, with positional restraints (10 kcal mol^{-1} $Å^{-2}$) on all heavy atoms; (ii) gradual heating from 0 to 300 K over 100 ps in the NVT ensemble with harmonic restraints on the solute; (iii) pressure equilibration for 500 ps in the NPT ensemble at 300 K and 1 bar, with restraints progressively reduced to zero. Production MD was then performed for 100 ns in the NPT ensemble at 300 K (Langevin thermostat, collision frequency 2 ps^{-1}) and 1 atm (Monte Carlo barostat). The SHAKE algorithm was applied to all bonds involving hydrogen, enabling a 2 fs integration timestep. Electrostatic interactions were treated using the particle mesh Ewald (PME) method with a real-space cutoff of 10 Å; the same cutoff was applied to van der Waals interactions. Coordinates were saved every 100 ps.

Trajectory analysis was performed using the CPPTRAJ module of AmberTools22. Backbone RMSD, per-residue RMSF, and radius of gyration (Rg) were calculated relative to the energy-minimized, equilibrated structure after superimposing each frame on the Cα atoms of the protein. All analyses were conducted over the full 100 ns production trajectory.

Binding free energies were estimated from the production trajectories using the molecular mechanics/generalized Born (and Poisson–Boltzmann) surface area approach (MM-GBSA/MM-PBSA) as implemented in the MMPBSA.py module of AmberTools22 [33,34]. Calculations used the single-trajectory protocol, extracting 101 evenly spaced frames from the final 60 ns of each AChE complex (Donepezil, **D4**, **D5**). The generalized Born model of Onufriev et al. [34] (igb = 2) was applied with an ionic strength of 0.15 M; the internal PBSA solver was used for the Poisson–Boltzmann calculations under the same ionic strength.

Entropic contributions were not computed, so the reported ΔG values are relative rather than absolute binding free energies.

2.5. Retrosynthetic Feasibility Assessment

Synthetic accessibility of the lead compounds was assessed at the route level using AiZynthFinder (v4.4.1) [35], an open-source retrosynthesis tool that performs a Monte Carlo tree search guided by a neural-network expansion policy trained on a USPTO-derived reaction-template library, recursively decomposing each target into commercially available precursors. The publicly distributed USPTO expansion and filter models were used, together with the ZINC purchasable-compound stock ($\approx 1.7 \times 10^7$ compounds). Canonical SMILES of the lead derivatives (**D4**, **D5**) were submitted individually; donepezil was processed under identical settings as a reference to confirm that the tool reproduces a known synthesis of the parent scaffold. For each target, the search returned ranked candidate routes, each annotated with a solved/unsolved status (whether all terminal precursors are present in the stock), the number of synthetic steps, and a route score. The top-ranked route for each compound was retained and rendered for inspection.

3. Results and Discussion

3.1. Compound Creation and Selection

A targeted approach for molecular generation and filtering described in the previous section was employed to design new Donepezil analogues that possess improved pharmacokinetic and safety profiles for the treatment of AD. To begin with, a total of 10,324 structurally diverse derivatives were produced through several iterations utilizing the CReM framework, where mutations were strategically introduced at non-critical positions of the Donepezil scaffold. The initial selection phase utilized removing duplicates (8143 left) and selecting according to drug-likeness criteria alongside medicinal chemistry filters, all while ensuring that synthetic accessibility remained at or below 4.5 and that the bioavailability score was favorable. The initial screening process narrowed the library down to 2341 potential candidates. A subsequent, more rigorous filtering phase focused on properties essential for CNS-active drugs, such as high predicted GI absorption, verified BBB permeation, and limited interaction with P-gp. Furthermore, we evaluated oral bioavailability, plasma protein binding, hepatotoxicity, hERG-related cardiotoxicity, as well as the mutagenic and carcinogenic potential, along with the profiles of CYP450 enzyme inhibition. A total of just 15 compounds successfully met the strict criteria established by this thorough ADMET-based selection process. Ultimately, cross-validation conducted through the SwissADME platform further honed the selection, resulting in 9 top-ranked derivatives for an in-depth comparative analysis with Donepezil.

Structures of the nine selected compounds are given in Figure 1.

3.2. ADMET Profile—Comparison with Donepezil

A diligent ADMET comparative analysis was conducted between Donepezil, the standard AChE inhibitor currently in clinical use, and the nine carefully chosen derivatives that have emerged from our computational screening process. The emphasis was placed on the physicochemical, pharmacokinetic, and toxicity parameters that are most pertinent to the design of drugs targeting the CNS.

From a physicochemical standpoint, Donepezil has a molecular weight (MW) of 379.21 g/mol, which falls comfortably within the range that allows for CNS permeability. Additionally, it features a topological polar surface area (TPSA) of 38.77 $Å^2$, representing a good balance for passive diffusion across the BBB. The logP value of 3.245 indicates a moderate level of lipophilicity, which aids in membrane permeability while maintaining

solubility, as evidenced by a logS of –3.866. In contrast, the derivatives exhibit higher molecular weights, ranging from 436.27 to 519.31 g/mol, while their TPSA values fall between 42.01 and 62.32 Å^2. The observed increases are still consistent with CNS delivery; however, a slight elevation in TPSA for certain derivatives (e.g., 59.08 and 62.32 Å^2) does not substantially hinder BBB permeation, as predicted probabilities remain above 0.92 for all compounds. Lipophilicity is notably reduced relative to Donepezil for several derivatives (logP 1.68–2.39 for **D5**–**D9**), which may enhance aqueous solubility and reduce off-target lipophilic interactions, while **D2** and **D3** show higher logP values (3.46–3.47).

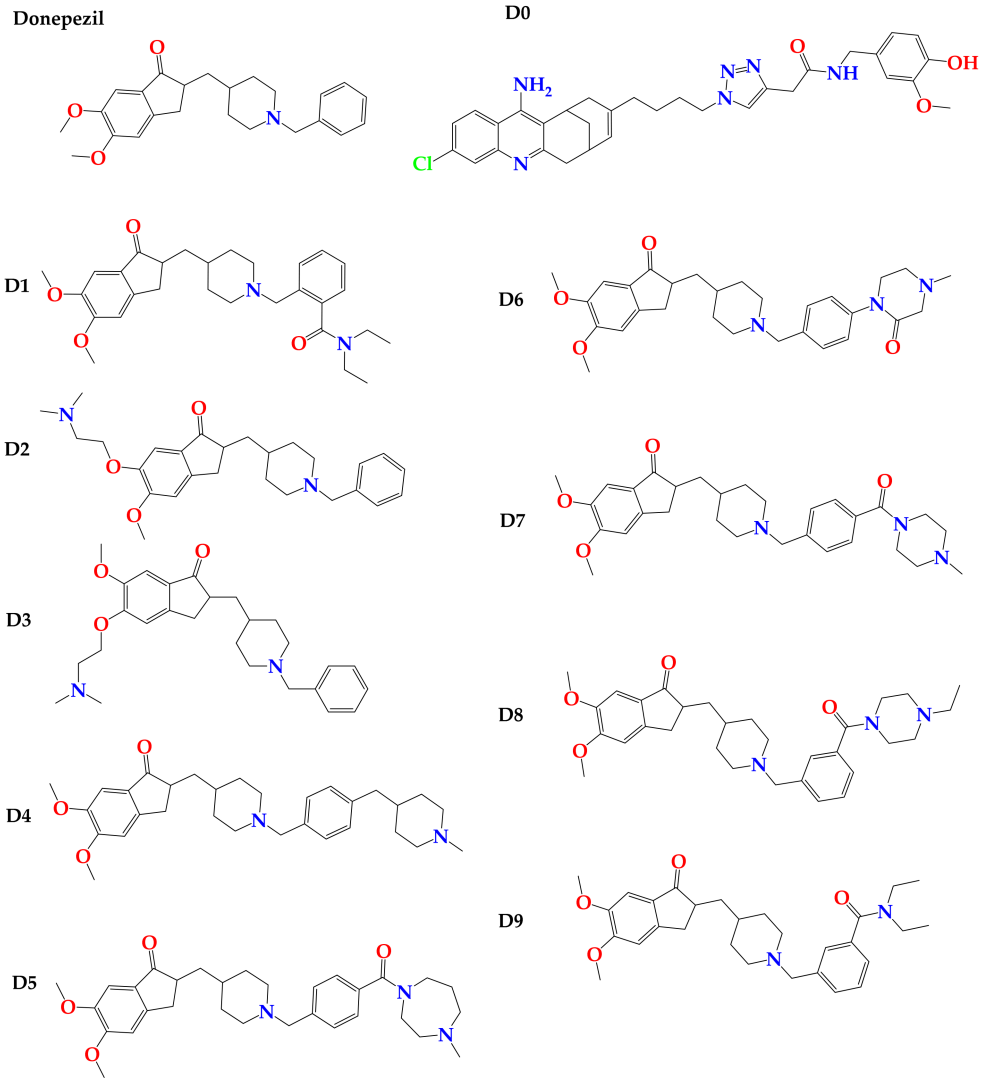


Figure 1. Structural representation of **D0**, Donepezil and its derivatives (**D1**–**D9**) obtained through CReM and selected according to ADMET profiles.

In the realm of medicinal chemistry metrics, Donepezil's Quantitative Estimate of Drug-likeness (QED) score of 0.747 indicates a strong drug-like profile. This is further validated by its adherence to the Lipinski, GSK, and Golden Triangle rules [36–38]. However, it does raise a flag with the Pfizer rule, attributed to its elevated logP and reduced TPSA. The derivatives exhibit somewhat lower QED values (0.506–0.589), indicating a rise in structural complexity and molecular weight; however, their synthetic accessibility scores (2.88–3.10) fall well within the practical limits for medicinal chemistry efforts. All derivatives successfully bypass PAINS and BRENK alerts, suggesting a minimal chance of assay interference.

Donepezil exhibits high predicted intestinal absorption, significant passive permeability in Caco-2 and MDCK cell models, strong P-glycoprotein inhibition (0.847), and low substrate liability (0.042). The derivatives show high predicted BBB penetration probabilities (0.923–0.990) alongside Human Intestinal Absorption (HIA) values below 2×10^{-4} across the series, suggesting adequate intestinal absorption. Taken together with favorable logP values (1.68–3.47), these predictions are consistent with CNS exposure, though experimental confirmation is required.

Donepezil binds extensively to plasma proteins (91.95%), which limits the free circulating fraction while extending half-life. Several derivatives show substantially lower predicted protein plasma binding (PPB) values (e.g., **D5**: 42.8%, **D7**: 42.9%, **D4**: 66.2%), which could increase the unbound circulating fraction, though whether this translates to greater CNS exposure would need experimental confirmation. All derivatives are predicted to be BBB-permeant (0.923–0.990). We note, however, that ADMETlab assigns Donepezil a low BBB probability (0.353) that conflicts both with its established clinical CNS activity and with the ProTox 3.0 prediction (0.99, Section Further Toxicological Profiling); this misprediction on a reference compound with an unambiguous clinical answer indicates that these probabilities should be read as qualitative permeant/non-permeant indicators rather than as a rank-ordering of CNS exposure. We therefore interpret the derivative values as consistent with BBB permeability, but not as evidence of superiority over Donepezil.

The toxicity profile reveals that Donepezil's significant risk of cardiotoxicity, indicated by a high hERG inhibition probability of 0.937, is reflected across the derivative series, with hERG values ranging from 0.955 to 0.998 (compounds **D2**, **D3**, and **D4** exceeding 0.990), warranting careful consideration. The predictions for neurotoxicity are notably elevated overall (Donepezil: 0.957; derivatives: 0.963–0.990), which aligns with the presence of strong CNS-active pharmacophores, yet underscores the need for focused toxicological assessments. However, some derivatives significantly enhance various safety margins, such as lowering the chances of hepatotoxicity and nephrotoxicity.

In summary, Donepezil's ADMET profile reflects a reasonably well-balanced combination of MW, TPSA, and logP for CNS penetration, though with notable predicted liabilities regarding hERG inhibition, CYP2D6-mediated interactions, and high PPB. The derivatives largely preserve predicted BBB penetration while showing opportunities for reduced PPB (notably **D5**, **D6**, and **D7**), improved solubility, and lower CYP2D6 inhibition in several analogues. Derivatives with lower predicted PPB, minimal CYP2D6 inhibition (notably **D5**–**D9**), and logP below 3 represent the candidates most worth prioritizing in subsequent experimental work.

These pharmacokinetic advantages are, however, compound-selective rather than general to the series, and are offset by higher molecular weight, lower QED (0.506–0.589 vs. 0.747), and predicted hERG and neurotoxicity liabilities comparable to or slightly greater than Donepezil. The derivatives therefore present a mixed profile rather than a uniform improvement. Derivatives combining the selective advantages with the fewest added liabilities—notably the lower-logP, lower-CYP2D6, lower-PPB subset **D5**–**D7**—represent the candidates most worth prioritizing in subsequent experimental work.

Further Toxicological Profiling

The extended toxicological assessment of the investigated derivatives was conducted using the ProTox 3.0 platform, with results benchmarked against donepezil. Predictions for acute oral toxicity placed the majority of compounds within toxicity class 4, with LD_{50} values ranging between 500 and 1000 mg/kg (**D1**: 900 mg/kg; **D2** and **D3**: 550 mg/kg; **D4**: 500 mg/kg; **D5**: 800 mg/kg; **D7**: 1000 mg/kg; **D8** and **D9**: 550 mg/kg), closely aligning with donepezil (505 mg/kg). Notably, compound **D6** was categorized as class 6 with an

LD_{50} of 6000 mg/kg, indicating a substantially lower predicted acute toxicity compared to both the reference and the remaining derivatives.

Predictions of organ-level toxicity indicated that hepatotoxicity, nephrotoxicity, and cardiotoxicity were consistently inactive across all derivatives, whereas neurotoxicity and respiratory toxicity emerged as recurrent concerns with probabilities ranging from 0.72 to 0.95. This pattern mirrors the donepezil profile, which was also predicted to be neurotoxic (0.90) and respiratory toxic (0.96). With respect to toxicity endpoints, all derivatives demonstrated low carcinogenic and mutagenic potential, with probabilities hovering near the inactive threshold (0.50–0.60). However, immunotoxicity was strongly predicted as active across the dataset (0.95–0.99), consistent with the reference compound (0.95), while clinical toxicity predictions fluctuated between borderline inactive and active (0.50–0.58), suggesting potential long-term safety liabilities.

Blood–brain barrier permeability was uniformly predicted as active for all compounds (0.73–0.95), in agreement with their intended central nervous system activity and closely reflecting the donepezil profile (0.99). Ecotoxicity predictions were largely inactive or borderline, although **D2**, **D3**, and **D4** exhibited slightly elevated values (0.58–0.59), warranting further consideration in environmental risk assessment.

At the molecular initiating event level, the majority of derivatives were predicted to retain interaction with AChE with high probability values (0.87–0.95), thereby corroborating the intended pharmacological mechanism. Other initiating events, including thyroid receptors, GABA and NMDA receptors, and PXR, were consistently inactive, thus reducing the likelihood of significant off-target neuroendocrine interactions.

Cytochrome P450 metabolism profiling suggested limited interference with major isoenzymes. The majority of compounds were predicted as inactive toward CYP1A2, CYP2C9, CYP2C19, and CYP2E1, while interactions with CYP3A4 were frequently predicted as active (0.59–0.66), suggesting potential metabolic liability via this isoform. In addition, derivatives **D2**, **D3**, and **D4** displayed predicted activity against CYP2D6 (0.76–0.78), a feature that may introduce inter-individual pharmacokinetic variability due to the well-established polymorphisms of this enzyme.

In summary, the toxicological profiles of the investigated derivatives largely recapitulate that of donepezil, most notably in terms of acute toxicity class, neurotoxicity, respiratory toxicity, immunotoxicity, and BBB penetration. Among them, **D6** distinguished itself by exhibiting a markedly improved predicted acute toxicity margin (LD_{50} = 6000 mg/kg) while preserving central nervous system accessibility and AChE interaction, thereby warranting prioritization in experimental follow-up. Nevertheless, the consistent prediction of immunotoxicity across the dataset emphasizes the need for careful experimental validation of immune-related liabilities prior to advancing these compounds into preclinical evaluation.

3.3. Molecular Docking—Inhibition of AChE and BChE

The docking process was carried out within grid boxes centered on the catalytic sites of AChE and BChE, designed to include the catalytic triad, the acyl-binding pocket, and the PAS. This setup guarantees that we address both the aromatic gorge and the surrounding contacts that are important for dual-site inhibition.

3.3.1. AChE—Affinity Landscape and Ligand Efficiency

All new ligands showed lower predicted binding free energies than donepezil, accompanied by reductions in calculated inhibitory constants (K*i*), as detailed in Table 1.

Table 1. Predicted molecular docking parameters for novel ligands and donepezil against acetylcholinesterase (AChE) and butyrylcholinesterase (BChE).

9.8			
Compound	**Binding Energy (kcal/mol)**	**Inhibitory Constant (nM)**	**Ligand Efficiency**
D1	−11.76	2.40	−0.34
D2	−12.29	0.98	−0.38
D3	−11.06	7.82	−0.35
D4	−13.41	0.15	−0.37
D5	−12.69	0.50	−0.33
D6	−12.55	0.63	−0.35
D7	−12.29	0.98	−0.33
D8	−13.08	0.26	−0.34
D9	−12.13	1.28	−0.35
Donepezil	−11.07	7.69	−0.40
D0	−11.66	2.84	−0.28
BChE			
Compound	**Binding Energy (kcal/mol)**	**Inhibitory Constant (nM)**	**Ligand Efficiency**
D1	−9.63	87.33	−0.28
D2	−9.98	48.37	−0.31
D3	−8.75	385.67	−0.27
D4	−11.00	8.65	−0.31
D5	−11.17	6.49	−0.29
D6	−10.30	28.19	−0.29
D7	−10.38	24.63	−0.28
D8	−9.95	50.89	−0.26
D9	−9.84	61.27	−0.28
Donepezil	−8.87	314.96	−0.32
D0	−10.61	16.70	−0.25

These docking-derived Ki values are score-based estimates intended for relative ranking and do not represent predicted absolute affinities; they are subject to the known limitations of empirical scoring functions and require experimental confirmation.

The highest-scoring compounds created the most stable complexes and demonstrated a "dual-site" binding mode, extending across the catalytic region and PAS via the aromatic gorge. The ligand efficiency (LE) values demonstrated consistency throughout the set and were marginally less negative than those of donepezil. This observation implies that the increase in absolute potency is partially attributed to enhanced packing and a larger contact surface (i.e., extension along the gorge), rather than being exclusively a result of per-atom interaction strength (Table 1).

3.3.2. BChE—Potential for Dual Inhibition

In BChE, the top-ranked candidates showed lower predicted ΔG values than the reference, with ligand efficiency values largely comparable to it (Table 1). We note that,

unlike the AChE complexes, the BChE predictions rest on docking alone and were not subjected to MD or MM-GBSA validation; they should therefore be read as preliminary and are not presented on the same evidential footing as the AChE results.

D0, the co-crystallized donepezil derivative present in the BChE reference structure, showed a more favorable predicted ΔG than donepezil, ranking above it in the series. Most of the nine novel ligands also showed lower predicted ΔG values than **D0**, with **D4** and **D5** among the strongest; based on the docking poses, this ranking is qualitatively associated with acyl-pocket occupancy and π–π contacts at the peripheral site. We describe these as relative rankings only: the docking-derived Ki values are not interpreted as quantitative affinity ratios, given the known limitations of empirical scoring functions. **D0** thus serves as a useful intermediate benchmark between donepezil and the current derivative series, pending dynamic validation of the BChE poses.

3.3.3. Selectivity: AChE Preference and "Balanced" Inhibitors

All ligands showed a preference for AChE over BChE in predicted binding, consistent with the extended contacts along the aromatic gorge and complementarity with the PAS (Table 1). Several compounds showed a relatively balanced profile across both enzymes, which is relevant given BChE's increasing role in advanced AD. **D0** showed a more balanced predicted profile than donepezil itself, attributable to improved hydrophobic fit within the BChE gorge. **D4** and **D5** showed lower predicted ΔG and K*i* values across both enzymes, consistent with combined acyl-pocket anchoring and π–π stacking toward the PAS. **D0** thus serves as a useful intermediate reference between donepezil and the current series.

3.3.4. Interaction Patterns—A Further Analysis of Molecular Docking Results

According to the literature, key characteristics of high-potency cholinesterase inhibitors are:

(i) a series of cooperative aromatic interactions (π–π and π–cation) that position the ligand along the gorge axis;
(ii) hydrogen bonds located near the catalytic triad and oxyanion hole that stabilize the polar head group or linker
(iii) the hydrophobic arrangement of terminal fragments within the acyl-binding pocket.

The docking interaction maps (Figures 2 and 3) showed that the new ligands interact extensively with the amino acid residues that control high-affinity cholinesterase binding. Top compounds like **D4**, **D8**, and **D5** created direct hydrogen bonds or polar interactions with the catalytic triad residues Ser203, His447, and Glu334, usually via carbonyl or heteroatom functions in the central scaffold. **D4** and **D8** formed stable hydrogen bonds to the oxyanion hole residues Gly121 and Gly122, anchoring the ligand's polar head group in the catalytic niche. All leading candidates in the aromatic gorge showed repeated π–π stacking interactions with Trp86 and Phe338. Tyr337 also commonly made π–π or π–alkyl connections. Furthermore, **D4** and **D8** connect to PAS residues (Tyr72, Asp74, and Tyr124) via π–π and hydrogen bonding interactions, confirming their dual-site binding mechanism. The hydrophobic tails of these ligands made contact with Phe295, Phe297, Leu289, and Val288 in the acyl-binding pocket, adding stability and binding energy.

Moreover, **D5** and **D4** hydrogen-bonded with Ser198 of the catalytic triad in BChE, whereas His438 and Glu325 indirectly contributed via the polar interaction network. Oxyanion hole residues Gly116 and Gly117 stabilized hydrogen bonds, especially for **D5**. The aromatic gorge residues Trp82, Tyr332, and Phe329 were consistently implicated in π–π or π–cation interactions, and **D5** had greater PAS engagement with Asp70 and Tyr332 than **D0**, the co-crystallized donepezil derivative. **D5**'s hydrophobic ends were anchored in the

acyl-binding pocket created by Leu286, Val288, Phe329, and Phe398, resulting in higher projected binding energy than **D0**.

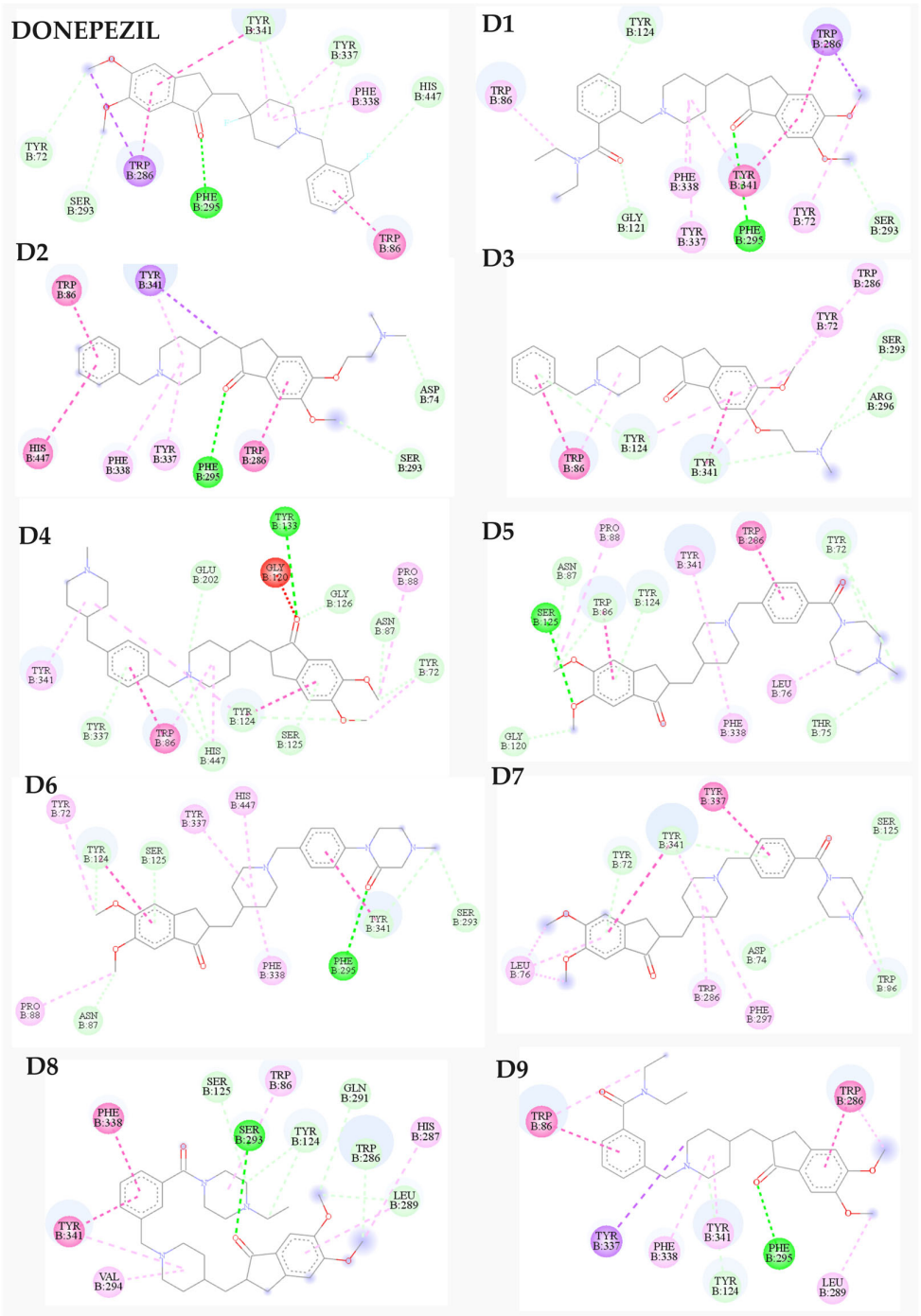


Figure 2. Predicted binding interactions of **D1**–**D9** within the active site of AChE. Interaction types are color-coded as follows: green—conventional hydrogen bonds; light green with dotted lines—carbon–hydrogen bonds; light green with no lines—Van der Waals interactions; pink—alkyl-alkyl and π–alkyl interactions; purple—π–π T–shaped and π–σ interactions; red—unfavorable interactions.

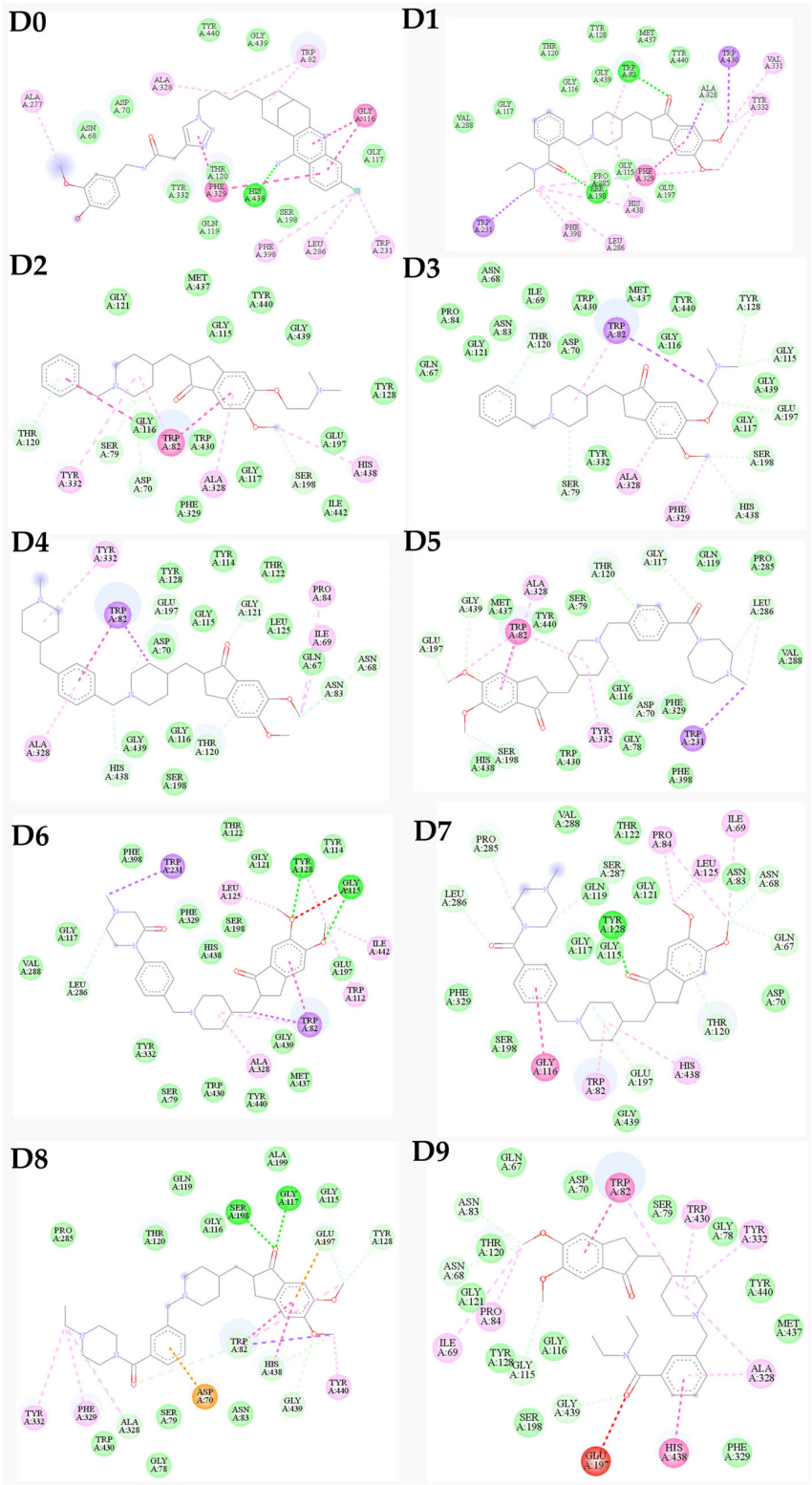


Figure 3. Predicted binding interactions of **D0**–**D9** within the active site of BChE. Interaction types are color-coded as follows: green—conventional hydrogen bonds; light green with dotted lines—carbon–hydrogen bonds; light green with no lines—Van der Waals interactions; pink—alkyl-alkyl and π–alkyl interactions; purple—π–π T–shaped and π–σ interactions; red—unfavorable interactions; yellow—π–anion interactions.

In summary, in AChE the highest-ranked ligands show a dual-site binding pattern spanning the catalytic site and PAS, while the leading BChE candidates exploit the wider active-site cavity with maintained catalytic site contacts, generally more effectively than **D0**.

The qualitative interaction patterns are consistent with the ranking in Table 1 and provide a plausible structural rationale for the observed differences in predicted affinity. These findings support prioritizing **D4** and **D5** for experimental follow-up, though docking-based predictions remain subject to the limitations of the scoring function and require confirmation by biochemical assay.

Overall, the docking results show a consistent trend of lower predicted ΔG values for the novel ligands relative to donepezil, with a predominant AChE preference and several candidates showing meaningful predicted BChE activity. **D4** and **D5** combine dual-site predicted binding with the lowest Ki values in both enzymes. The mechanistic interpretation—dual-site anchoring, π-stacking along the gorge, and hydrophobic acyl-pocket contacts—is internally consistent with the numerical ranking in Table 1 and with literature data on high-affinity cholinesterase inhibitors. These data provide a computational rationale for selecting **D4** and **D5** as primary candidates for synthesis and in vitro evaluation.

3.4. Molecular Dynamics Simulations Analysis

To further validate the stability of the docking-predicted binding poses, 100 ns molecular dynamics (MD) simulations were performed for the two top-ranked candidates, **D4** and **D5**, in complex with AChE, using Donepezil as the reference. Three independent metrics were monitored throughout: the backbone root-mean-square deviation (RMSD) relative to the energy-minimized starting structure, the per-residue root-mean-square fluctuation (RMSF), and the radius of gyration (Rg) of the protein.

3.4.1. RMSD and Conformational Stability

All three systems reached conformational equilibrium within approximately 10 ns and remained stable thereafter (Figure 4). Over the full 100 ns trajectory, the Donepezil–AChE complex displayed a mean backbone RMSD of 1.44 ± 0.14 Å, with a plateau in the last 50 ns at 1.51 ± 0.08 Å. **D4** exhibited a mean RMSD of 1.47 ± 0.22 Å (last 50 ns: 1.62 ± 0.11 Å), and **D5** showed a slightly higher mean of 1.59 ± 0.22 Å (last 50 ns: 1.71 ± 0.12 Å). All values remained well below the 2.0 Å threshold commonly considered indicative of conformational drift, confirming that the ligand-bound complexes are stable throughout the simulation window. The marginally elevated RMSD for **D5** relative to Donepezil reflects the larger molecular volume of this derivative and the associated minor rearrangements of peripheral loops, rather than any disruption of the binding mode.

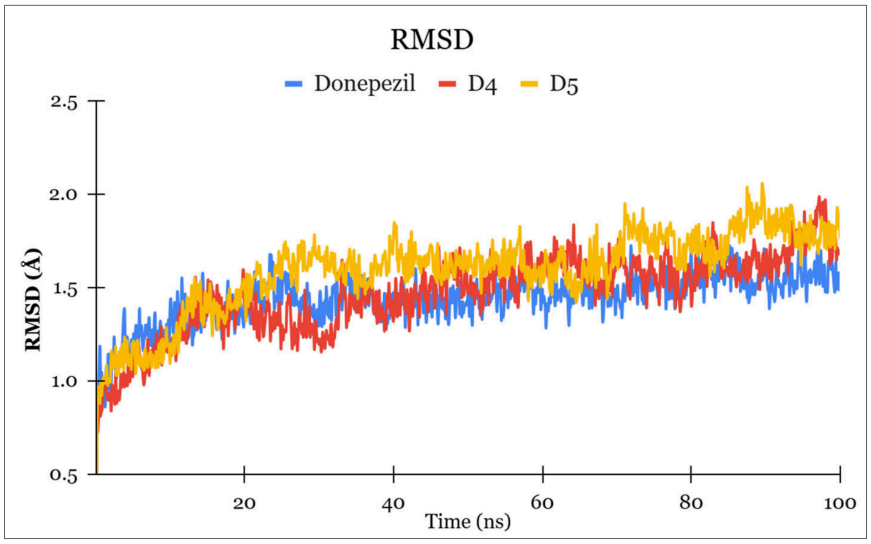


Figure 4. Backbone RMSD of the AChE–ligand complexes over 100 ns of MD simulation for Donepezil, **D4**, and **D5**.

3.4.2. RMSF and Residue-Level Flexibility

Per-residue RMSF profiles were overall comparable across the three systems (Figure 5), with mean fluctuations of 0.95 ± 0.49 Å for Donepezil, 1.02 ± 0.54 Å for **D4**, and 1.02 ± 0.54 Å for **D5**. Elevated fluctuations localized to terminal and surface-exposed loops (residues 1–2, ~257–260, ~380–384, and ~484–489) were present in all three systems and are a hallmark of AChE surface mobility unrelated to the active-site gorge.

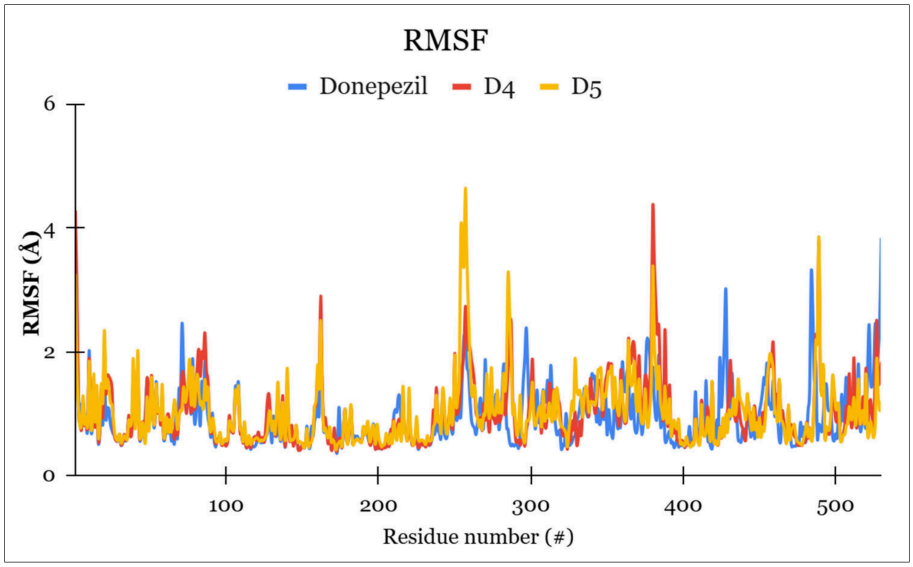


Figure 5. Per-residue RMSF of AChE backbone atoms over 100 ns of MD simulation for Donepezil, **D4**, and **D5**. Key binding site residues are indicated.

Critically, the residues that define high-affinity cholinesterase binding were consistently rigid. The catalytic triad (Ser203, His447, Glu334) showed RMSF values below 1.0 Å in all three complexes, confirming that ligand binding does not perturb the catalytic machinery. Oxyanion hole residues Gly121 and Gly122 fluctuated below 0.7 Å across all systems. PAS residues Tyr72, Asp74, and Tyr124 displayed RMSF values in the 0.53–1.74 Å range, with **D4** and **D5** showing slightly reduced fluctuations compared to Donepezil at Tyr72 (**D4**: 1.62 Å; **D5**: 1.43 Å vs. Donepezil: 1.74 Å) and Tyr124 (**D4**: 0.61 Å; **D5**: 0.56 Å vs. Donepezil: 0.53 Å), consistent with tighter PAS engagement of the derivatives as suggested by the docking results. Notable differences were observed at acyl-binding pocket residues Phe295 and Phe297, where Donepezil showed substantially higher fluctuations (1.52 and 2.38 Å, respectively) compared to **D4** (0.65 and 0.73 Å) and **D5** (0.59 and 0.86 Å), indicating that the extended scaffolds of **D4** and **D5** provide more effective hydrophobic anchoring in this region.

3.4.3. Radius of Gyration and Structural Compactness

The Rg of the AChE backbone (Figure 6) remained stable across all simulations, confirming that ligand binding does not induce global unfolding or domain rearrangements. The Donepezil complex maintained a mean Rg of 22.745 ± 0.057 Å throughout the simulation (last 50 ns: 22.773 ± 0.048 Å). The **D4** and **D5** complexes showed slightly but consistently higher Rg values (**D4**: 22.923 ± 0.096 Å; **D5**: 22.974 ± 0.108 Å), with a gradual upward drift in the second half of the trajectory (**D4** last 50 ns: 22.986 ± 0.068 Å; **D5** last 50 ns: 23.054 ± 0.063 Å). This modest increase in Rg (~0.3 Å) is well within the range of normal thermal fluctuation and simply reflects the larger molecular volume of the derivatives occupying the binding gorge, rather than any loss of structural compactness. Consistent with this, the RMSF data (Section 3.4.2) show that elevated per-residue fluctuations are

confined to peripheral, surface-exposed loops unrelated to the active-site gorge, while the catalytic, oxyanion-hole, and PAS residues remain rigid. The overall protein fold is therefore preserved in both derivative complexes.

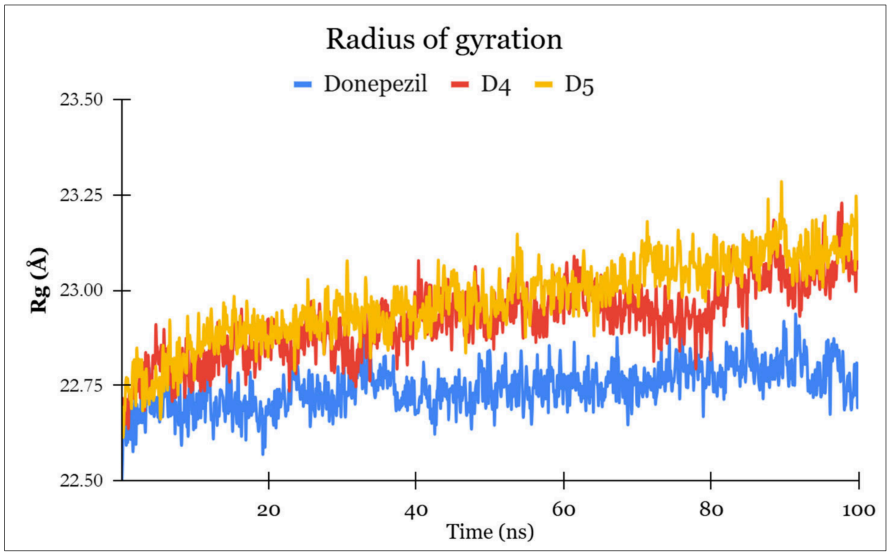


Figure 6. Radius of gyration (Rg) of the AChE backbone over 100 ns of MD simulation for Donepezil, **D4**, and **D5**.

Taken together, the MD data corroborate and extend the static docking results. The binding poses of **D4** and **D5** are dynamically stable over a 100 ns timescale, the catalytic and PAS residues critical for dual-site inhibition maintain low flexibility in both derivative complexes, and the acyl-binding pocket is more effectively anchored by **D4** and **D5** than by Donepezil itself. These findings strengthen the case for prioritizing **D4** and **D5** in subsequent experimental validation.

3.4.4. Binding Free Energy (MM-GBSA/MM-PBSA)

To move beyond docking-score ranking, MM-GBSA and MM-PBSA binding free energies were computed over the final 60 ns of each AChE trajectory using the MMPBSA.py module of AmberTools22. MM-GBSA yielded ΔG_bind values of -28.9 ± 0.3 (Donepezil), -36.7 ± 0.4 (**D4**), and -30.0 ± 0.4 (**D5**) kcal/mol, identifying **D4** as the strongest binder, in agreement with the docking ranking; **D5** was comparable to Donepezil within error. MM-PBSA absolute values were positive (Donepezil +12.8, **D4** +10.9, **D5** +10.5 kcal/mol), a known consequence of overestimation of the polar desolvation term by the internal PBSA solver for cationic ligands; these are therefore interpreted only as relative estimates, and likewise place both derivatives at or below Donepezil. Entropic contributions were not included, so the values are relative rather than absolute affinities. Taken together, the free-energy data support the docking-based prioritization of **D4** while indicating that **D5**'s advantage over Donepezil is method-dependent and modest.

3.5. Synthetic Feasibility

The CReM platform is specifically engineered to generate chemically reasonable and synthetically accessible derivatives, as evidenced by the synthetic accessibility scores (SAscore ≤ 4.5) for all selected candidates (**D1–D9**). However, CReM generates chemically reasonable mutations but does not guarantee synthetic tractability or novelty of any individual analogue, and the fragment library constrains the accessible chemical space. This threshold indicates that the proposed modifications remain practical for laboratory synthesis using standard organic reactions. To complement these composite scores with

route-level evidence, retrosynthetic analyses were performed for the lead compounds using AiZynthFinder, a neural-network-guided Monte Carlo tree-search tool that recursively breaks a target down to purchasable precursors using a USPTO-derived reaction-template library. As a validation of the parent chemotype, the tool reproduced the established aldol-type synthesis of donepezil from 5,6-dimethoxy-1-indanone and N-benzylpiperidine-4-carbaldehyde. For **D5**, a fully solved three-step convergent route was identified in which all four precursors are commercially available, combining the same aldol condensation used for donepezil, an amide coupling between 4-(bromomethyl)benzoic acid and 1-methyl-1,4-diazepane, and an N-alkylation joining the two arms. For **D4**, a three-step convergent route was likewise proposed in which three of the four precursors are commercially available; the sole out-of-stock precursor is formaldehyde, a ubiquitous reagent excluded only by the drug-like scope of the precursor database rather than by genuine unavailability. Both derivatives share the dimethoxyindanone and benzylpiperidine building blocks of donepezil, indicating that they are accessible through established synthetic logic. These routes are computational proposals; experimental synthesis and structural confirmation remain necessary.

While the in silico results are encouraging at the computational level, they require experimental validation before any pharmacological conclusion can be drawn.

3.6. Limitations and Required Experimental Validation

The present study is entirely computational, and its conclusions are predictions rather than demonstrated pharmacological properties. Several limitations should be made explicit. (i) All binding metrics—docking ΔG, docking-derived Ki, and MM-GBSA/MM-PBSA free energies—are computational estimates; the docking-derived Ki values in particular are score-based and are not reliable estimators of absolute affinity, and the MM-PBSA absolute values are affected by the known overestimation of the polar desolvation term. These support relative ranking, not absolute potency. (ii) MD simulations were run as single 100 ns trajectories without independent replicas, and only for the AChE complexes; the BChE predictions rest on docking alone. (iii) ADMET and toxicity endpoints derive from QSAR-type classifiers whose reliability depends on training-set coverage, as illustrated by the ADMETlab misprediction of Donepezil's BBB permeability. (iv) The derivatives present a mixed safety profile, retaining Donepezil's predicted hERG and neurotoxicity liabilities and adding a consistently predicted immunotoxicity and CYP3A4 interaction. Accordingly, the following must be established experimentally before any candidate advances: synthesis and structural confirmation of the leads; in vitro AChE/BChE inhibition (Ellman method, IC_{50}); BBB permeability (PAMPA-BBB and/or MDCK-MDR1); direct CYP inhibition assays (with attention to CYP3A4 and CYP2D6); hERG patch-clamp; microsomal metabolic stability; cytotoxicity in neuronal and hepatic lines; and cell-based Aβ-aggregation assays. Extension of the MD and MM-PBSA analysis to the BChE complexes is a further defined computational step.

4. Conclusions

Using fragment-based molecular design (CReM), AI-assisted retrosynthetic assessment, multi-parameter ADMET screening, molecular docking, and MD simulations, we computationally identified nine Donepezil derivatives with predicted CNS-relevant pharmacokinetics, a mixed toxicity profile in which selective improvements (e.g., hepatotoxicity, nephrotoxicity, CYP2D6) are offset by retained hERG and neurotoxicity liabilities, and improved docking scores for dual AChE/BChE inhibition. **D4** and **D5** showed the most favorable predicted binding profiles, with dual-site poses in AChE and MD-stable complexes over 100 ns. **D6** is notable for a substantially higher predicted LD_{50} than the remaining

derivatives and donepezil. The scaffolds are synthetically accessible (SAscore $\leq$ 4.5) and represent plausible candidates for experimental follow-up. Route-level retrosynthetic analysis (AiZynthFinder) further supported synthetic feasibility, returning a fully solved three-step route for **D5** and a near-complete route for **D4** from largely commercial precursors, both sharing donepezil's core building blocks. Whether these computational predictions translate to measurable inhibitory activity remains to be determined by synthesis and in vitro assay.

Supplementary Materials: The following supporting information can be downloaded at: https://www.mdpi.com/article/10.3390/compounds6030045/s1, Figure S1: Redocking validation of the docking protocol. Superposition of the co-crystallized (crystal) and redocked poses of donepezil in the acetylcholinesterase active site (PDB 4EY7). The redocked pose reproduces the crystallographic binding mode with a heavy-atom RMSD of 1.96 Å, confirming the reliability of the docking protocol; Figure S2; Predicted three-dimensional binding poses of the lead derivatives D4 and D5 in the acetylcholinesterase gorge (PDB 4EY7). Key active-site residues are shown, illustrating simultaneous engagement of the catalytic site and the peripheral anionic site (PAS) that underlies the proposed dual-site binding. Dashed lines indicate predicted interactions; Figure S3; Predicted retrosynthetic routes for the lead derivatives, generated with AiZynthFinder. (A) Donepezil, reproduced as validation of the tool on the parent scaffold. (B) D5, a fully solved three-step convergent route from four commercially available precursors. (C) D4, a three-step convergent route in which three of four precursors are commercially available. Green boxes denote precursors present in the purchasable-compound stock; Table S1: SwissADME-predicted physicochemical, pharmacokinetic, drug-likeness, and medicinal chemistry profile of donepezil and derivatives D1–D9; Table S2: ADMETlab 3.0-predicted absorption, distribution, metabolism, excretion, toxicity, and safety endpoints of donepezil and derivatives D1–D9.

Author Contributions: Conceptualization, M.A. and M.S.P.; methodology, J.Đ.J.; software, S.J.; validation, M.A., M.G. and A.A.; formal analysis, A.A.; investigation, S.J.; resources, M.A.; data curation, J.Đ.J.; writing—original draft preparation, M.A.; writing—review and editing, M.S.P.; visualization, M.G.; supervision, A.A. All authors have read and agreed to the published version of the manuscript.

Funding: This research was funded by the Serbian Ministry of Education, Science, and Technological Development (Agreement Nos 451-03-33/2026-03/200378; 451-03-34/2026-03/200111 and 451-03-137/2025-03/200252).

Data Availability Statement: The original contributions presented in this study are included in the article/Supplementary Material. Further inquiries can be directed to the corresponding author.

Acknowledgments: During the preparation of this manuscript/study, the author(s) used the CReM (Chemically Reasonable Mutations) https://crem.readthedocs.io (accessed on 17 July 2026) algorithm for the generation of structurally feasible derivatives of the parent compound, and AIZynthFinder (v4.4.1) for retrosynthetic analysis. Claude (Anthropic) (v2.1) and ChatGPT (OpenAI) (v5.4) were used for language and style assistance, specifically for improving sentence structure and grammatical accuracy of the manuscript. The authors have reviewed and edited the output and take full responsibility for the content of this publication.

Conflicts of Interest: The authors declare no conflicts of interest. The funders had no role in the design of the study; in the collection, analyses, or interpretation of data; in the writing of the manuscript; or in the decision to publish the results.

Abbreviations

The following abbreviations are used in this manuscript:

AD	Alzheimer's disease
ACh	Acetylcholine
AChE	Acetylcholinesterase
BChE	Butyrylcholinesterase
Aβ	Beta-amyloid peptide
PAS	Peripheral anionic site
CNS	Central nervous system
CReM	Chemically Reasonable Mutations
ADMET	Absorption, Distribution, Metabolism, Excretion, and Toxicity
GI	Gastrointestinal
BBB	Blood–brain barrier
P-gp	P-glycoprotein
PPB	Plasma protein binding
CYP	Cytochrome P450
hERG	Human Ether-à-go-go-Related Gene potassium channel
HIA	Human intestinal absorption
Ki	Inhibitory constant
ΔG	Binding free energy
LE	Ligand efficiency
MW	Molecular weight
TPSA	Topological polar surface area
logP	Partition coefficient
logS	Aqueous solubility
QED	Quantitative Estimate of Drug-likeness
PAINS	Pan-Assay Interference Compounds
BRENK	Structural alerts filter
LGA	Lamarckian Genetic Algorithm
MMFF94	Merck Molecular Force Field
PDB	Protein Data Bank

References

1. Frank, E.M. Effect of Alzheimer's disease on communication function. *J. S. C. Med. Assoc.* **1994**, *90*, 417–423. [PubMed]
2. Gatz, M.; Reynolds, C.A.; Fratiglioni, L.; Johansson, B.; Mortimer, J.A.; Berg, S.; Fiske, A.; Pedersen, N.L. Role of genes and environments for explaining Alzheimer disease. *Arch. Gen. Psychiatry* **2006**, *63*, 168–174. [CrossRef] [PubMed]
3. Rodriguez, S.; Thiruchelvi, R.; Thenmozhi, A.J.; Cosio, D.S.; Shamaladevi, N.; Hussain, H.; Kumar, S.; Rajasekar, N.; Manivasagam, T.; Essa, M.M. Fat and Alzheimer's Disease. In *Nutraceuticals for Alzheimer's Disease: A Promising Therapeutic Approach*; Essa, M.M., Akbar, M., Manivasagam, T., Eds.; Springer: Singapore, 2023; pp. 67–89.
4. Rondeau, V.; Commenges, D.; Jacqmin-Gadda, H.; Dartigues, J.-F. Relation between Aluminum Concentrations in Drinking Water and Alzheimer's Disease: An 8-year Follow-up Study. *Am. J. Epidemiol.* **2000**, *152*, 59–66. [CrossRef] [PubMed]
5. Lin, J.N.; Lin, C.L.; Lin, M.C.; Lai, C.H.; Lin, H.H.; Yang, C.H.; Kao, C.H. Increased Risk of Dementia in Patients with Acute Organophosphate and Carbamate Poisoning: A Nationwide Population-Based Cohort Study. *Medicine* **2015**, *94*, e1187. [CrossRef] [PubMed]
6. Plassman, B.L.; Havlik, R.J.; Steffens, D.C.; Helms, M.J.; Newman, T.N.; Drosdick, D.; Phillips, C.; Gau, B.A.; Welsh–Bohmer, K.A.; Burke, J.R.; et al. Documented Head Injury in Early Adulthood and Risk of Alzheimer's Disease and Other Dementias. *Neurology* **2000**, *55*, 1158–1166. [CrossRef] [PubMed]
7. Huang, Q.; Liao, C.; Ge, F.; Ao, J.; Liu, T. Acetylcholine Bidirectionally Regulates Learning and Memory. *J. Neurorestoratol.* **2022**, *10*, 100002. [CrossRef]
8. Mesulam, M.M.; Geula, C. Butyrylcholinesterase Reactivity Differentiates the Amyloid Plaques of Aging from Those of Dementia. *Ann. Neurol.* **1994**, *36*, 722–727. [CrossRef] [PubMed]
9. Ballard, C.; Greig, N.; Guillozet-Bongaarts, A.; Enz, A.; Darvesh, S. Cholinesterases: Roles in the Brain During Health and Disease. *Curr. Alzheimer Res.* **2005**, *2*, 307–318. [CrossRef] [PubMed]

10. Furukawa-Hibi, Y.; Alkam, T.; Nitta, A.; Matsuyama, A.; Mizoguchi, H.; Suzuki, K.; Moussaoui, S.; Yu, Q.-S.; Greig, N.H.; Nagai, T.; et al. Butyrylcholinesterase Inhibitors Ameliorate Cognitive Dysfunction Induced by Amyloid-β Peptide in Mice. *Behav. Brain Res.* **2011**, *225*, 222–229. [CrossRef] [PubMed]
11. Ahmed, M.; Davis, J.; Aucoin, D.; Sato, T.; Ahuja, S.; Aimoto, S.; Elliott, J.I.; Van Nostrand, W.E.; Smith, S.O. Structural Conversion of Neurotoxic Amyloid-β1–42 Oligomers to Fibrils. *Nat. Struct. Mol. Biol.* **2010**, *17*, 561–567. [CrossRef] [PubMed]
12. Hardy, J.; Bogdanovic, N.; Winblad, B.; Portelius, E.; Andreasen, N.; Cedazo-Minguez, A.; Zetterberg, H. Pathways to Alzheimer's Disease. *J. Intern. Med.* **2014**, *275*, 296–303. [CrossRef] [PubMed]
13. Cleary, J.; Walsh, D.; Hofmeister, J.; Shankar, G.M.; Kuskowski, M.; Selkoe, D.J. Natural Oligomers of the Amyloid-β Protein Specifically Disrupt Cognitive Function. *Nat. Neurosci.* **2005**, *8*, 79–84. [PubMed]
14. De Ferrari, G.V.; Canales, M.A.; Shin, I.; Weiner, L.M.; Silman, I.; Inestrosa, N.C. A Structural Motif of Acetylcholinesterase That Promotes Amyloid β-Peptide Fibril Formation. *Biochemistry* **2001**, *40*, 10447–10457. [CrossRef] [PubMed]
15. Makhaeva, G.F.; Kovaleva, N.V.; Boltneva, N.P.; Rudakova, E.V.; Lushchekina, S.V.; Astakhova, T.Y.; Serkov, I.V.; Proshin, A.N.; Radchenko, E.V.; Palyulin, V.A.; et al. Bis-Amiridines as Acetylcholinesterase and Butyrylcholinesterase Inhibitors: N-Functionalization Determines the Multitarget Anti-Alzheimer's Activity Profile. *Molecules* **2022**, *27*, 1060. [CrossRef] [PubMed]
16. Polishchuk, P. CReM: Chemically Reasonable Mutations. Available online: https://crem.readthedocs.io (accessed on 17 July 2026).
17. Baell, J.B.; Holloway, G.A. New Substructure Filters for Removal of Pan Assay Interference Compounds (PAINS) from Screening Libraries and for Their Exclusion in Bioassays. *J. Med. Chem.* **2009**, *52*, 3101–3107.
18. Daina, A.; Zoete, V.; Banerjee, P.; Michielin, O. SwissADME: A Free Web Tool to Evaluate Pharmacokinetics, Drug-Likeness and Medicinal Chemistry Friendliness of Small Molecules. *Sci. Rep.* **2017**, *7*, 42717. [CrossRef] [PubMed]
19. Fu, L.; Shi, S.; Yi, J.; Wang, N.; He, Y.; Wu, Z.; Peng, J.; Deng, Y.; Wang, W.; Wu, C.; et al. ADMETlab 3.0: An Updated Comprehensive Online ADMET Prediction Platform Enhanced with Broader Coverage, Improved Performance, API Functionality and Decision Support. *Nucleic Acids Res.* **2024**, *52*, W422–W431. [CrossRef] [PubMed]
20. Morris, G.M.; Huey, R.; Lindstrom, W.; Sanner, M.F.; Belew, R.K.; Goodsell, D.S.; Olson, A.J. AutoDock4 and AutoDockTools4: Automated Docking with Selective Receptor Flexibility. *J. Comput. Chem.* **2009**, *30*, 2785–2791. [CrossRef] [PubMed]
21. Santos-Martins, D.; Forli, S.; Ramos, M.J.; Olson, A.J. AutoDock Multi-Target Docking (AMDock): A Graphical Tool for AutoDock4. *Bioinformatics* **2021**, *37*, 4455–4457. [CrossRef] [PubMed]
22. Cheung, J.; Rudolph, M.J.; Burshteyn, F.; Cassidy, M.S.; Gary, E.N.; Love, J.; Franklin, M.C.; Height, J.J. Structures of human acetylcholinesterase in complex with pharmacologically important ligands. *J. Med. Chem.* **2012**, *55*, 10282–10286. [CrossRef] [PubMed]
23. Viayna, E.; Coquelle, N.; Cieslikiewicz-Bouet, M.; Cisternas, P.; Oliva, C.A.; Sanchez-Lopez, E.; Ettcheto, M.; Bartolini, M.; De Simone, A.; Ricchini, M.; et al. Discovery of a Potent Dual Inhibitor of Acetylcholinesterase and Butyrylcholinesterase with Antioxidant Activity that Alleviates Alzheimer-like Pathology in Old APP/PS1 Mice. *J. Med. Chem.* **2021**, *64*, 812–839. [PubMed]
24. Halgren, T.A. Merck Molecular Force Field. I. Basis, Form, Scope, Parameterization, and Performance of MMFF94. *J. Comput. Chem.* **1996**, *17*, 490–519. [CrossRef]
25. Dassault Systèmes BIOVIA. *Discovery Studio Visualizer*, version 21.1.0; Dassault Systèmes: San Diego, CA, USA, 2021. Available online: https://www.3ds.com/products/biovia/discovery-studio/visualization (accessed on 17 July 2026).
26. Wan, D.; Wang, F.-Q.; Xie, J.; Chen, L.; Zhou, X.-L. Design, synthesis, and biological activity of donepezil: Aromatic amine hybrids as anti-Alzheimer's drugs. *ACS Omega* **2023**, *8*, 21802–21812. [CrossRef] [PubMed]
27. PubChem. 2-{1-[4-(12-Amino-3-chloro-6,7,10,11-tetrahydro-7,11-methanocycloocta[b]quinolin-9-yl)butyl]-1H-1,2,3-triazol-4-yl}-N-[4-hydroxy-3-methoxybenzyl]acetamide, CID 156612856. Available online: https://pubchem.ncbi.nlm.nih.gov/compound/156612856 (accessed on 17 July 2026).
28. Hopkins, A.L.; Groom, C.R.; Alex, A. Ligand Efficiency: A Useful Metric for Lead Selection. *Drug Discov. Today* **2004**, *9*, 430–431. [CrossRef] [PubMed]
29. Jo, S.; Kim, T.; Iyer, V.G.; Im, W. CHARMM-GUI: A web-based graphical user interface for CHARMM. *J. Comput. Chem.* **2008**, *29*, 1859–1865. [CrossRef] [PubMed]
30. Maier, J.A.; Martinez, C.; Kasavajhala, K.; Wickstrom, L.; Hauser, K.E.; Simmerling, C. ff14SB: Improving the accuracy of protein side chain and backbone parameters from ff99SB. *J. Chem. Theory Comput.* **2015**, *11*, 3696–3713. [CrossRef] [PubMed]
31. Wang, J.; Wolf, R.M.; Caldwell, J.W.; Kollman, P.A.; Case, D.A. Development and Testing of a General Amber Force Field. *J. Comput. Chem.* **2004**, *25*, 1157–1174. [CrossRef] [PubMed]
32. He, X.; Man, V.H.; Yang, W.; Lee, T.-S.; Wang, J. A Fast and High-Quality Charge Model for the Next Generation General AMBER Force Field. *J. Chem. Phys.* **2020**, *153*, 114502. [CrossRef] [PubMed]
33. Case, D.A.; Aktulga, H.M.; Belfon, K.; Ben-Shalom, I.Y.; Berryman, J.T.; Brozell, S.R.; Cerutti, D.S.; Cheatham, T.E., III; Cisneros, G.A.; Cruzeiro, V.W.D.; et al. *AMBER 22*; University of California: San Francisco, CA, USA, 2022. Available online: https://ambermd.org/doc12/Amber22.pdf (accessed on 17 July 2026).

34. Genheden, S.; Thakkar, A.; Chadimová, V.; Reymond, J.-L.; Engkvist, O.; Bjerrum, E. AiZynthFinder: A Fast, Robust and Flexible Open-Source Software for Retrosynthetic Planning. *J. Cheminform.* **2020**, *12*, 70. [CrossRef] [PubMed]
35. Miller, B.R., III; McGee, T.D., Jr.; Swails, J.M.; Homeyer, N.; Gohlke, H.; Roitberg, A.E. MMPBSA.py: An Efficient Program for End-State Free Energy Calculations. *J. Chem. Theory Comput.* **2012**, *8*, 3314–3321. [CrossRef] [PubMed]
36. Lipinski, C.A.; Lombardo, F.; Dominy, B.W.; Feeney, P.J. Experimental and Computational Approaches to Estimate Solubility and Permeability in Drug Discovery and Development Settings. *Adv. Drug Deliv. Rev.* **1997**, *23*, 3–25. [CrossRef]
37. Leeson, P.D.; Springthorpe, B. The Influence of Drug-like Concepts on Decision-Making in Medicinal Chemistry. *Nat. Rev. Drug Discov.* **2007**, *6*, 881–890. [CrossRef] [PubMed]
38. Johnson, T.W.; Dress, K.R.; Edwards, M. Using the Golden Triangle to optimize clearance and oral absorption. *Bioorganic Med. Chem. Lett.* **2009**, *19*, 5560–5564. [CrossRef] [PubMed]

Disclaimer/Publisher's Note: The statements, opinions and data contained in all publications are solely those of the individual author(s) and contributor(s) and not of MDPI and/or the editor(s). MDPI and/or the editor(s) disclaim responsibility for any injury to people or property resulting from any ideas, methods, instructions or products referred to in the content.